The influence of non-imaging detector design on heralded ghost-imaging and ghost-diffraction examined using a triggered ICCD camera

D. S. Tasca,[1,*] **R. S. Aspden,**[1,4] **P. A. Morris,**[1] **G. Anderson,**[1] **R. W. Boyd,**[2,3] **and M. J. Padgett**[1]

[1]*SUPA, School of Physics and Astronomy, University of Glasgow, Glasgow, G12 8QQ, UK*
[2]*Institute of Optics, University of Rochester, Rochester, NY 14627, USA*
[3]*Department of Physics, University of Ottawa, Ottawa, ON K1N 6N5, Canada*
[4]*r.aspden.1@research.gla.ac.uk*
[*]*tasca@if.ufrj.br*

Abstract: Ghost imaging and ghost diffraction can be realized by using the spatial correlations between signal and idler photons produced by spontaneous parametric down-conversion. If an object is placed in the signal (idler) path, the spatial correlations between the transmitted photons as measured by a single, non-imaging, "bucket" detector and a scanning detector placed in the idler (signal) path can reveal either the image or diffraction pattern of the object, whereas neither detector signal on its own can. The details of the bucket detector, such as its collection area and numerical aperture, set the number of transverse modes supported by the system. For ghost imaging these details are less important, affecting mostly the sampling time required to produce the image. For ghost diffraction, however, the bucket detector must be filtered to a single, spatially coherent mode. We examine this difference in behavour by using either a multi-mode or single-mode fibre to define the detection aperture. Furthermore, instead of a scanning detector we use a heralded camera so that the image or diffraction pattern produced can be measured across the full field of view. The importance of a single mode detection in the observation of ghost diffraction is equivalent to the need within a classical diffraction experiment to illuminate the aperture with a spatially coherent mode.

OCIS codes: (270.0270) Quantum optics; (190.4420) Nonlinear optics, transverse effects in; (040.1490) Cameras; (030.5260) Photon counting.

References and links

1. T. B. Pittman, Y. H. Shih, D. V. Strekalov, and A. V. Sergienko, "Optical imaging by means of two-photon quantum entanglement," Phys. Rev. A **52**, R3429–R3432 (1995).
2. D. V. Strekalov, A. V. Sergienko, D. N. Klyshko, and Y. H. Shih, "Observation of two-photon "ghost" interference and diffraction," Phys. Rev. Lett. **74**, 3600–3603 (1995).
3. A. Gatti, E. Brambilla, M. Bache, and L. A. Lugiato, "Ghost imaging with thermal light: Comparing entanglement and classical correlation," Phys. Rev. Lett. **93**, 093602 (2004).
4. F. Ferri, D. Magatti, A. Gatti, M. Bache, E. Brambilla, and L. A. Lugiato, "High-resolution ghost image and ghost diffraction experiments with thermal light," Phys. Rev. Lett. **94**, 183602 (2005).

#198207 - $15.00 USD Received 23 Sep 2013; revised 4 Nov 2013; accepted 4 Nov 2013; published 4 Dec 2013

5. T. Iskhakov, A. Allevi, D. A. Kalashnikov, V. G. Sala, M. Takeuchi, M. Bondani, and M. Chekhova, "Intensity correlations of thermal light," Eur. Phys. J. Special Topics **199**, 127–138 (2011).
6. G. Brida, M. V. Chekhova, G. A. Fornaro, M. Genovese, E. D. Lopaeva, and I. R. Berchera, "Systematic analysis of signal-to-noise ratio in bipartite ghost imaging with classical and quantum light," Phys. Rev. A **83**, 063807 (2011).
7. R. S. Aspden, D. S. Tasca, R. W. Boyd, and M. J. Padgett, "EPR-based ghost imaging using a single-photon-sensitive camera," New J. Phys. **15**, 073032 (2013).
8. P. H. S. Ribeiro, S. Pádua, J. C. Machado da Silva, and G. A. Barbosa, "Controlling the degree of visibility of Young's fringes with photon coincidence measurements," Phys. Rev. A **49**, 4176–4179 (1994).
9. P. H. Souto Ribeiro and G. A. Barbosa, "Direct and ghost interference in double-slit experiments with coincidence measurements," Phys. Rev. A **54**, 3489–3492 (1996).
10. S. P. Walborn, P. H. Souto Ribeiro, and C. H. Monken, "Interference effects induced by non-local spatial filtering," Opt. Express **19**, 17308–17317 (2011).
11. J. O. de Almeida, S. P. Walborn, P. H. Souto Ribeiro, and M. Hor-Meyll, "Fourth-order coherence induced by spatial mode parity selection," Phys. Rev. A **86**, 033839 (2012).
12. R. Fickler, M. Krenn, R. Lapkiewicz, S. Ramelow, and A. Zeilinger, "Real-time imaging of quantum entanglement," Sci. Rep. **3**, 1914 (2013).
13. C. H. Monken, P. H. Souto Ribeiro, and S. Pádua, "Transfer of angular spectrum and image formation in spontaneous parametric down-conversion," Phys. Rev. A **57**, 3123–3126 (1998).
14. M. D'Angelo, M. V. Chekhova, and Y. Shih, "Two-photon diffraction and quantum lithography," Phys. Rev. Lett. **87**, 013602 (2001).
15. A. F. Abouraddy, P. R. Stone, A. V. Sergienko, B. E. A. Saleh, and M. C. Teich, "Entangled-photon imaging of a pure phase object," Phys. Rev. Lett. **93**, 213903 (2004).
16. I. F. Santos, L. Neves, G. Lima, C. H. Monken, and S. Pádua, "Generation and detection of magnified images via illumination by entangled photon pairs," Phys. Rev. A **72**, 033802 (2005).
17. M. B. Nasr, D. P. Goode, N. Nguyen, G. Rong, L. Yang, B. M. Reinhard, B. E. A. Saleh, and M. C. Teich, "Quantum optical coherence tomography of a biological sample," Opt. Commun. **282**, 1154–1159 (2009).
18. S. P. Walborn, C. H. Monken, S. Pádua, and P. H. Souto Ribeiro, "Spatial correlations in parametric down-conversion," Phys. Rep. **495**, 87–139 (2010).
19. S. P. Walborn, A. N. de Oliveira, S. Padua, and C. H. Monken, "Multimode Hong-Ou-Mandel interference," Phys. Rev. Lett. **90**, 143601 (2003).
20. C. K. Law and J. H. Eberly, "Analysis and interpretation of high transverse entanglement in optical parametric down conversion," Phys. Rev. Lett. **92**, 127903 (2004).
21. E. Yao, S. Franke-Arnold, J. Courtial, M. J. Padgett, and S. M. Barnett, "Observation of quantum entanglement using spatial light modulators," Opt. Express **14**, 13089–13094 (2006).
22. V. D. Salakhutdinov, E. R. Eliel, and W. Löffler, "Full-field quantum correlations of spatially entangled photons," Phys. Rev. Lett. **108**, 173604 (2012).
23. M. Krenn, R. Fickler, M. Huber, R. Lapkiewicz, W. Plick, S. Ramelow, and A. Zeilinger, "Entangled singularity patterns of photons in Ince-Gauss modes," Phys. Rev. A **87**, 012326 (2013).
24. N. A. Peters, J. T. Barreiro, M. E. Goggin, T.-C. Wei, and P. G. Kwiat, "Remote state preparation: Arbitrary remote control of photon polarization," Phys. Rev. Lett. **94**, 150502 (2005).
25. M. A. Solís-Prosser and L. Neves, "Remote state preparation of spatial qubits," Phys. Rev. A **84**, 012330 (2011).
26. Y. Kang, K. Cho, J. Noh, D. L. P. Vitullo, C. Leary, and M. G. Raymer, "Remote preparation of complex spatial states of single photons and verification by two-photon coincidence experiment," Opt. Express **18**, 1217–1233 (2010).
27. A. M. Brańczyk, T. C. Ralph, W. Helwig, and C. Silberhorn, "Optimized generation of heralded Fock states using parametric down-conversion," New J. Phys. **12**, 063001 (2010).
28. F. M. Miatto, H. D. L. Pires, S. M. Barnett, and M. P. van Exter, "Spatial Schmidt modes generated in parametric down-conversion," Eur. Phys. J. D **66**, 263 (2012).
29. F. M. Miatto, T. Brougham, and A. M. Yao, "Cartesian and polar Schmidt bases for down-converted photons: How high dimensional entanglement protects the shared information from non-ideal measurements," Eur. Phys. J. D **66**, 183 (2012).
30. S. P. Walborn and A. H. Pimentel, "Generalized Hermite–Gauss decomposition of the two-photon state produced by spontaneous parametric down conversion," J. Phys. B: At. Mol. Opt. Phys. **45**, 165502 (2012).
31. J. C. Howell, R. S. Bennink, S. J. Bentley, and R. W. Boyd, "Realization of the Einstein-Podolsky-Rosen paradox using momentum- and position-entangled photons from spontaneous parametric down conversion," Phys. Rev. Lett. **92**, 210403 (2004).
32. P. H. S. Ribeiro, C. H. Monken, and G. A. Barbosa, "Measurement of coherence area in parametric downconversion luminescence," Appl. Opt. **33**, 352–355 (1994).
33. E. Lantz, J.-L. Blanchet, L. Furfaro, and F. Devaux, "Multi-imaging and Bayesian estimation for photon counting with EMCCDs," Mon. Not. R. Astron. Soc. **386**, 2262–2270 (2008).
34. D. S. Tasca, M. P. Edgar, F. Izdebski, G. S. Buller, and M. J. Padgett, "Optimizing the use of detector arrays for

#198207 - $15.00 USD Received 23 Sep 2013; revised 4 Nov 2013; accepted 4 Nov 2013; published 4 Dec 2013

measuring intensity correlations of photon pairs," Phys. Rev. A **88**, 013816 (2013).
35. C. H. Sequin, "Blooming suppression in charge coupled area imaging devices," Bell Syst. Tech. J. **51**, 1923 (1972).

1. Introduction

Nearly 20 years ago, Pittman *et al.* [1] and Strekalov *et al.* [2] published their seminal papers on ghost imaging and ghost diffraction using spatially correlated photons produced by spontaneous parametric down-conversion (SPDC). In ghost imaging [1], the object is illuminated by one of the down-converted beams, and a single-pixel detector is used to detect the transmitted photons. A spatially resolving detector is placed in the path of the other down-converted beam. The signals from neither of these detectors themselves can produce an image of the object, yet the correlations between them yields an image. In essence, a transmitted photon in the object beam is position-correlated with its paired photon in the other beam, the position of which is recorded by the scanning detector. In a similar work performed by the same group [2] they were able to extend this concept to ghost diffraction where, if placed in the far field, the scanning detector could reveal the diffraction pattern of the object rather than its image.

Being based on photon pairs produced by SPDC, it was natural to assume that these phenomena were a manifestation of quantum mechanics. However, it is now recognized that many of the results in ghost imaging and diffraction can be replicated using classical sources. The uniquely quantum aspect is that background-free ghost imaging and ghost diffraction can be performed with the same apparatus where imaging and diffraction are manifestations of transverse position and transverse momentum correlations of the photon pairs [3, 4]. Within the classical approach for ghost imaging and diffraction, it is possible to work with correlated light sources in the intense light regime, for which intensity correlation measurements can be performed using standard CCD arrays [4–6]. In the quantum configuration, however, it is of course necessary to make measurements on single-photons belonging to a correlated pair produced by the SPDC source, placing technological requirements on the quantum efficiency of the detectors.

We have recently reported a technological advance in single-photon ghost imaging, where the scanning detector was replaced by a time-gated camera capable of measuring over the full field of view [7]. This eliminates the need for sequential scanning and increases the optical efficiency of the ghost imaging system proportional to the number of pixels in the image. In the present paper we extend this work to consider the additional requirements needed to perform ghost diffraction. Whereas ghost imaging requires only correlations in the source, ghost diffraction places additional constraints upon the detection.

When performing any simple diffraction experiment, a high contrast diffraction pattern is obtained only when the object is illuminated with a spatially coherent source. Within a ghost configuration this is equivalent to the detection of the photons transmitted by the object in a spatially coherent mode, whilst noting that the scanning/imaging detector in the other beam remains unchanged. The degree of visibility of fourth-order diffraction and interference patterns has been investigated by varying the collection area of the non-imaging single-pixel detector [8–11]. In this work, we illustrate this restriction by fibre coupling the single-pixel detector used to collect the photons transmitted by the object. If a single mode fibre is used, then it is possible to perform both ghost imaging and ghost diffraction. If, however, the fibre is multimode, the ghost diffraction pattern is no longer visible.

As discussed, the use of a camera rather than a scanning detector gives an increase in optical efficiency compared to previous works. This image-based coincidence detection system [7, 12] is a versatile tool for applications in fourth-order imaging techniques [13–17] and for the study of spatial correlations of photons.

#198207 - $15.00 USD Received 23 Sep 2013; revised 4 Nov 2013; accepted 4 Nov 2013; published 4 Dec 2013

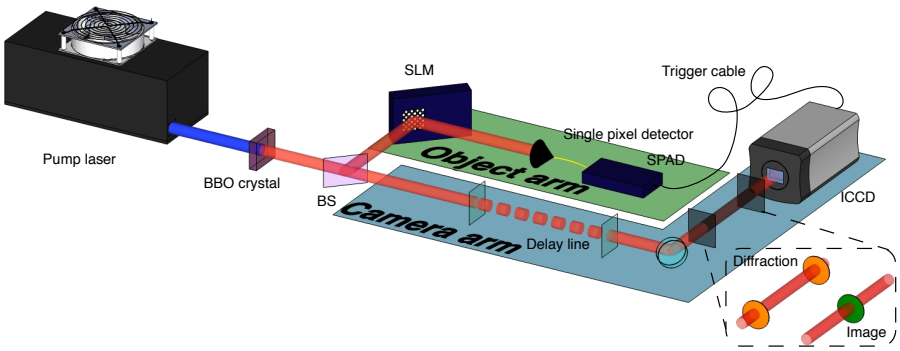

Fig. 1. Experimental setup. A type-I phase matched SPDC source emits frequency degenerate down-converted photons in a collinear configuration. The generated photon pairs are probabilistically split at the beam splitter (BS) and propagate through the object and camera arms. The detections of the photons in the object arm are used as a trigger for the acquisitions of the ICCD. Ghost images or diffraction patterns of the object encoded on the spatial light modulator (SLM) are obtained on the ICCD.

2. Theoretical background

We consider the two-photon state produced by spontaneous parametric down-conversion in a thin non-linear crystal set for collinear type-I phase-matching. By selecting the correlated photon pairs at the degenerate wavelength by the use of narrow band interference filters, the spatial structure of the two-photon field can be described by a pure state $|\Psi\rangle$ as

$$|\Psi\rangle = \int\int d\rho_s\, d\rho_i\, \Psi(\rho_s,\rho_i)|\rho_s\rangle|\rho_i\rangle, \tag{1}$$

where ρ_s and ρ_i are the transverse coordinates for signal and idler photons at the SPDC source and $|\rho\rangle$ represent a pure state of a single-photon in the transverse position ρ. The transverse mode function $\Psi(\rho_s,\rho_i)$ is non-separable and is written as an Einstein-Podolsky-Rosen like wave function of the form [18–20]

$$\Psi(\rho_s,\rho_i) = \mathscr{W}(\rho_s+\rho_i)\Gamma(\rho_s-\rho_i), \tag{2}$$

where $\mathscr{W}$ is the transverse profile of the pump beam and Γ is the Fourier transform of the phase-matching function. By using a pump beam with a relatively large Gaussian transverse profile, the transverse mode function is entangled over a wide range of spatial modes [20].

Let the generated photon pairs described by the state (1) propagate through the optical system depicted in Fig. 1. Frequency-degenerate photon pairs are emitted in a collinear configuration and are probabilistically split at the beam splitter (BS). We name the transmitted and reflected output paths of the BS as the *camera arm* and the *object arm*, respectively. An imaging system characterized by magnification M is placed in both arms. Considering only the case where the photons are split at the BS, the propagated transverse mode function of the two-photon field can be written as

$$\Psi'(\rho_1,\rho_2) = \frac{i}{2}\left[\Psi\left(\frac{\rho_1}{M},\frac{\rho_2}{M}\right)+\Psi\left(\frac{\rho_2}{M},\frac{\rho_1}{M}\right)\right], \tag{3}$$

where $\rho_1 = (x_1,y_1)$ and $\rho_2 = (x_2,y_2)$ are the transverse coordinates in the object and camera arm, respectively, and a $50:50$ beam splitter is assumed. Note that the inversion of the horizontal coordinate, x, caused by the reflection at the BS is neglected, as it is compensated for by

#198207 - $15.00 USD Received 23 Sep 2013; revised 4 Nov 2013; accepted 4 Nov 2013; published 4 Dec 2013

further reflections in the optical system. The two terms in Eq. (3) represent the two possibilities in which signal and idler photons are split into different paths at the BS.

The photons in the object arm are incident on a spatial light modulator (SLM) placed in the image plane of the SPDC source. The SLM is programmed to perform an amplitude modulation on the transverse profile of the photons, so its effect can be described by an aperture function $A(\rho_1)$. A microscope objective lens collects the photons diffracted from the SLM, and is adjusted to focus a collimated light beam onto the input facet of a single- or multi-mode optical fibre. When using a single-mode fibre in the detection system, the photons diffracted from the SLM are projected into a single transverse spatial mode ψ_{mn} that can be selected by the use of different holograms on the SLM [21–23]. In this case, the effect of the SLM in conjunction with the detection of the photon by the single-mode fibre can be described by the measurement operator

$$\hat{\Pi}_{SM} = |\phi_{mn}\rangle\langle\phi_{mn}|, \tag{4}$$

where the state $|\phi_{mn}\rangle$ is written as

$$|\phi_{mn}\rangle = \int d\rho_1 A(\rho_1)\psi_{mn}(\rho_1)|\rho_1\rangle. \tag{5}$$

Here ψ_{mn} is a square-integrable two-dimensional function whose indices m and n are associated with orthogonal transverse degrees of freedom such as the cartesian coordinates x and y or the polar coordinates given by the azimuthal angle and the radial position.

The detection of a photon in the object arm heralds the presence of a photon in the camera arm, whose state is prepared according to the measurement performed on its correlated partner [24–27]. By projecting the photon in the object arm in the pure state given in Eq. (5), the correlated photon in the camera arm is prepared in a pure state $|\chi_{mn}\rangle_2$ given by

$$|\chi_{mn}\rangle_2 \propto {}_1\langle\phi_{mn}|\Psi\rangle = \int d\rho_2 \chi_{mn}(\rho_2)|\rho_2\rangle, \tag{6}$$

where the mode function $\chi_{mn}(\rho_2)$ is given by the overlap integral

$$\chi_{mn}(\rho_2) = \int d\rho_1\, A(\rho_1)\psi^*_{mn}(\rho_1)\Psi'(\rho_1,\rho_2). \tag{7}$$

Here $\Psi'(\rho_1,\rho_2)$ is the propagated transverse mode function (3) of the two-photon state and it is assumed that the aperture function is real: $A = A^*$. For an idealized EPR state, the two-particle wave-function is written as a delta function, $\Psi_{EPR}(\rho_1,\rho_2) = \delta(\rho_1-\rho_2)$. Considering the two-photon transverse mode function (2), this corresponds to a limit of infinitely large transverse pump profile $\mathscr{W}$ and infinitely thin non-linear crystal. In this limit case, the transverse mode function of the heralded state (6) is given by $\chi_{mn}(\rho_2) = A(\rho_2)\psi^*_{mn}(\rho_2)$, which is the complex conjugate of the mode function in which the photon in the object arm is projected, and thus is modulated by the object's aperture function A. In our experiment, the mode function ψ_{mn} in which the projection is made is a fundamental Gaussian mode, ψ_G, and the overlap integral (7) can be calculated from the mode decomposition of the SPDC transverse wave-function (2) for a Gaussian pump beam: $\int d\rho_1 \Psi(\rho_1,\rho_2)\psi_G(\rho_1) \propto \psi_G(\rho_2)$ [see, for example, [28–30]]. The heralded state (6) of the photon in the camera arm based on the Gaussian projection of the trigger photon is given by a pure state whose transverse mode function is modulated by the object's aperture function

$$|\chi_G\rangle_2 \propto \int d\rho_2 A(\rho_2)\psi^*_G(\rho_2)|\rho_2\rangle. \tag{8}$$

On the other hand, the use of a large core diameter multi-mode fibre enables the detection of the full set of transverse modes diffracted from the SLM. The detection operator associated with

#198207 - $15.00 USD Received 23 Sep 2013; revised 4 Nov 2013; accepted 4 Nov 2013; published 4 Dec 2013

the multi-mode fibre can be written as a sum of the measurement operator (4) over a complete set of modes

$$\hat{\Pi}_{MM} = \sum_{m,n} \hat{\Pi}_{SM} = \sum_{m,n} |\phi_{mn}\rangle\langle\phi_{mn}| = \int d\rho_1 A^2(\rho_1)|\rho_1\rangle\langle\rho_1|, \tag{9}$$

where we used $\sum_{m,n} \psi_{mn}(\rho)\psi^*_{mn}(\rho') = \delta(\rho-\rho')$ with $\{\psi_{mn}\}$ being a complete set of orthogonal functions described by discrete indices m and n spanning the transverse mode space of the photons. In this case, the heralded photon in the camera arm is prepared in a mixed state $\hat{\varsigma}_2$ given by [24]

$$\begin{aligned} \hat{\varsigma}_2 \propto \mathrm{Tr}_1(\hat{\Pi}_{MM}|\Psi\rangle\langle\Psi|) &= \sum_{m,n} |\chi_{mn}\rangle\langle\chi_{mn}| \\ &= \int d\rho_2 \int d\rho_2' \left[\int d\rho_1 A^2(\rho_1)\,\Psi'(\rho_1,\rho_2)\Psi'^*(\rho_1,\rho_2')\right] |\rho_2\rangle\langle\rho_2'|, \end{aligned} \tag{10}$$

where Tr_1 is the partial trace with respect to the photon 1 in the object arm. In the following we will calculate the detection probabilities for the heralded states (8) and (10) in the camera arm.

2.1. Detection probabilities on the ICCD camera

In the transmitted path of the BS, the photons propagate through a system of lenses and are detected on the ICCD. The acquisitions of the ICCD are triggered by the detection of a photon in the object arm, such that photons detected on the ICCD and in the object arm belong to the same generated pair. The overall propagation distance from the SPDC source to the ICCD is 22.8m, and was chosen to compensate for the electronic delay of the trigger mechanism [7]. The ICCD is placed either in the image or Fourier plane of the SPDC source, each configuration selected by means of interchangeable lens systems. The magnification of the camera arm imaging system, M, is equivalent to that of the object arm, whereas the Fourier system is characterized by an effective focal length f_e. In both configurations, the ICCD provides a multi-pixel detection system capable of measuring the full transverse field of the down-converted light in the camera arm.

When the acquisitions of the ICCD are triggered based on the detection of the correlated photon with the single-mode fibre, the detection probabilities can be calculated from the pure heralded state given in Eq. (8). By positioning the ICCD in the image plane (IP) or far-field (FF) of the SPDC source, the detection probabilities are

$$\mathscr{P}_{SM,IP}(\rho_2) \propto |\langle\rho_2|\chi_G\rangle_2|^2 = A^2(\rho_2)|\psi_G(\rho_2)|^2, \tag{11}$$

and

$$\mathscr{P}_{SM,FF}(\rho_2) \propto |\langle k\rho_2/f_e|\chi_G\rangle_2|^2 = \left|\int d\xi\, \tilde{A}(\xi)\tilde{\psi}_G\left(\frac{k}{f_e}\rho_2 - \xi\right)\right|^2 \approx \left|\tilde{A}\left(\frac{k}{f_e}\rho_2\right)\right|^2, \tag{12}$$

respectively, where $k = 2\pi/\lambda$ is the wavenumber of the down-converted photons. The functions $\tilde{A}$ and $\tilde{\psi}_G$ are, respectively, the Fourier transform of the object's aperture function A and the Gaussian mode ψ_G coupled into the single-mode fibre. The Gaussian mode ψ_G is defined at the plane of the SLM, and its size is set by the microscope objective lens used to couple the light on the SLM into the single-mode fibre. By adjusting this coupling such that $\tilde{\psi}_G$ is very narrow, we can approximate Eq. (12) by the Fourier transform of the aperture function.

Using the trigger from the multi-mode detection system, we calculate the detection probabilities on the ICCD from the heralded state given by Eq. (10). The detection probabilities at the image plane and far-field of the SPDC source are

$$\mathscr{P}_{MM,IP}(\rho_2) \propto \int d\rho_1 A^2(\rho_1)|\Psi'(\rho_1,\rho_2)|^2 \approx A^2(\rho_2)|\Psi'(\rho_1=\rho_2,\rho_2)|^2, \tag{13}$$

#198207 - $15.00 USD Received 23 Sep 2013; revised 4 Nov 2013; accepted 4 Nov 2013; published 4 Dec 2013

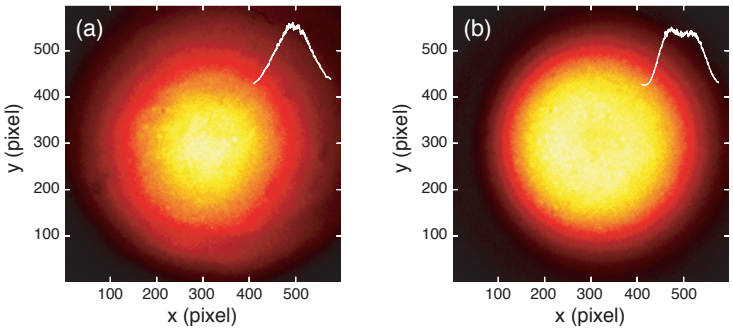

Fig. 2. (a) Near-field and (b) far-field patterns of the down-converted light as seen on the ICCD camera. The insets show a cross-section of the beam. These images are the result of summing 10 acquisitions of 1s each with the intensifier fired continuously.

and

$$\mathscr{P}_{MM,FF}(\rho_2) \propto \int d\rho_1 A^2(\rho_1) \left| \int d\rho_2' \Psi'(\rho_1,\rho_2') \exp\left(i\frac{k}{f_e}\rho_2\rho_2'\right)\right|^2, \tag{14}$$

respectively.

The down-converted photon pairs display a strong position correlation and momentum anti-correlation [31]. With the ICCD positioned in the image plane of the SPDC source, the photo-detection position is correlated with the position of the trigger photon at the plane of the SLM, reflecting in the detection probabilities (11) and (13) being shaped by the object's aperture function A and generating a ghost image of the object. Detecting the trigger photons with a single-mode fibre modulates the ghost image on the ICCD with the gaussian mode ψ_G. On the other hand, the use of the multi-mode fibre is equivalent to a bucket detector that is able to detect the full set of modes transmitted through the aperture [1, 7]. In this case, the object's aperture function is modulated by the full down-converted light intensity, generating a ghost image on the ICCD with contributions from the full set of transverse modes.

Although the detection probabilities in the far-field using both the single-mode (12) and multi-mode (14) detection systems contain information about the object's aperture function, its diffraction pattern $|\tilde{A}|^2$ is only visible when using a single-mode detection at the object arm. The detection probability (12) is given by the convolution of the Fourier transform of the object's aperture function and the Gaussian distribution of the detection mode. This is a typical diffraction pattern generated by a single-mode illumination of an aperture. On the other hand, the detection probability (14) is equivalent to the diffraction pattern of an aperture illuminated with an incoherent superposition of multiple transverse spatial modes. The resulting detection probability in this case is the sum of the diffraction patterns generated from each transverse mode.

3. Experimental setup

Our correlated photon imaging and diffraction experiment is based on spatially entangled photons from SPDC and a triggered multi-pixel detection system [7], as illustrated in Fig. 1. The spatially entangled photons are produced by a type-I phase-matched SPDC source using a 3mm long β-barium borate (BBO) crystal pumped by a high-repetition rate laser at $\lambda_p = 355$nm producing near-collinear propagating, frequency degenerate down-converted photons at $\lambda = 710$nm that are selected by the use of 10nm wide band-pass interference filters.

#198207 - $15.00 USD Received 23 Sep 2013; revised 4 Nov 2013; accepted 4 Nov 2013; published 4 Dec 2013

The output of the pump laser (a JDSU Xcyte Series pulsed laser with pulse width of 10ps and repetition rate of 100MHz) is spatially filtered to produce fundamental Gaussian beam with a diameter of approximately 1.3mm (FWHM). We use an imaging system with magnification $M = 3$ to produce an image of the output field of the SPDC source onto the SLM (in the object arm) and onto the input plane of an image preserving delay-line (in the camera arm). These imaging systems comprise of a 100mm focal length lens placed between the BBO crystal and the BS and two 300mm focal length lenses placed between the BS and the SLM and between the BS and the input plane of the delay line (DL). Both the SLM and the input plane of the DL are located at 80cm from the BBO crystal.

The illumination pattern used to probe the SLM is a 3 times magnified image of the output field provided by the SPDC source. This is a spatially incoherent [32], multi-mode beam with a diameter of $\approx$ 4mm (FWHM). Our SLM is a LCOS-SLM from Hamamatsu with an array of 600×800 pixels of size 20μm. The SLM is programmed to produce an amplitude modulation with the shape of a chess board, *i.e.* a pattern of alternate opaque and transparent squares. The aperture function $A(\rho_1)$ associated with this modulation assumes only the values "0" or "1", such that $A^2 = A = A^*$. The side length of each square is 300μm, corresponding to 15 pixels of the SLM. The output light of the SLM is collected by a $\times 4$ microscope objective lens and focused onto the input facet of an optical fibre connected to a single-photon avalanche diode (SPAD).

The counts registered in the SPAD indicate the detection of photons diffracted from the SLM but give no information about the object $A(\rho_1)$. We use the electronic output signal from the SPAD to trigger an acquisition of the ICCD camera placed in the camera arm [7, 12]. The ICCD (Andor iStar 334T with a generation 3 image intensifier) is operated in direct gate mode, meaning that the gate duration of the intensifier is set by the length of the trigger pulse ($\approx$ 15ns). In order to detect photons belonging to the same generated pair, the trigger of the intensifier on the ICCD must be synchronized with the arrival of the correlated photon on the ICCD. As demonstrated in [7], the delay of our triggering mechanism is approximately 70ns, which we compensate by means of a 22m long delay line in the camera arm. The delay-line consists of a number of consecutive telescopic imaging systems with unity magnification, imaging the transverse spatial distribution of the photons from the input to the output plane of the DL, and is represented in Fig. 1 by the dashed line in the camera arm. Thus, by properly adjusting the length of the cables from the SPAD to the ICCD, we are able to detect the photons whose correlated partners have been detected by the SPAD.

A switchable lens system is used after the DL to re-image or to Fourier transform the down-converted field at the output plane of the DL onto the ICCD. The transformation from the SPDC source to the ICCD is characterized either by an imaging system with magnification $M = 3$ or a Fourier system with an effective focal length of $f_e \approx 167$mm. Using the ICCD camera, we recorded images of the down-converted light in the image plane and the far-field of the SPDC source, as shown in Fig. 2. These images were acquired using the internal trigger of the ICCD to gate the intensifier continuously (10 acquisitions of 1s each), thus revealing the intensity pattern of the SPDC light. As shown in Fig. 2, the diameter of the down-converted beam as seen on the ICCD is approximately the same in both configurations. The illumination pattern used to probe the SLM in the object arm is equivalent to the distribution shown in Fig. 2(a).

4. Experimental results

Using the settings described in the previous section, we acquired 1800 triggered images on the ICCD for each of the four configurations (single- and multi-mode fibre with the ICCD in the image plane and far-field). Each image was acquired over a $\tau = 2$s exposure, resulting in a total acquisition time of 1 hour. We work with a region of interest (ROI) on the ICCD comprising

#198207 - $15.00 USD Received 23 Sep 2013; revised 4 Nov 2013; accepted 4 Nov 2013; published 4 Dec 2013

600×600 pixels operating in the single-photon counting regime; applying a binary threshold to the pixel outputs of each acquisition [7, 33, 34] and summing the resulting pixel intensities over all acquired images. As the pixel size of the CCD chip is 13μm, the field of view of the selected ROI is $(7.8 \times 7.8)\text{mm}^2$. Figure 3 shows the resulting images using the single-mode fibre (3-a and 3-b) and multi-mode fibre (3-c and 3-d). Horizontal cross-sections of the acquired images are shown in Fig. 4. The displayed cross-sections were averaged over the 20 central rows for the images taken in the image plane and over the 120 central rows for the images taken in the far-field.

Figure 5 shows a 200×200 pixels enlargement of the central part of the acquired images.With the ICCD positioned at the image plane, ghost images of the chess board pattern are obtained using both the single-mode, Fig. 3(a), or the multi-mode, Fig. 3(c), detection system. On the other hand, with the ICCD positioned in the far field, a diffraction pattern of the chess board is visible only when using the single-mode detection system in the object arm, Fig. 3(b). As shown in section 2, these images correspond to the detection probabilities of the heralded states (8) and (10) in the image plane and far-field of the SPDC source. The single-mode detection of the trigger photons in the object arm prepares the pure heralded state (8), whose detection probabilities in the image plane and far-field of the SPDC source are given in Eq. (11) and (12), respectively. The intensity pattern of the image shown in Fig. 3(a) [see also Fig. 5(a)] is given by the object's aperture function modulated by the intensity profile of the Gaussian mode in which the trigger photons are projected, as described in Eq. (11). By placing the ICCD in the far-field of the SPDC source, we record the image shown in Fig. 3(b) [see also Fig. 5(b)], which correspond to the convolution of the Fourier transforms of the object's aperture function and of the Gaussian detection mode.

The trigger detection system with the multi-mode fibre (core diameter of 400μm) acts as a bucket detector, collecting all the light transmitted through the object. The heralded state (10) prepared based on this detection is an incoherent sum of the single down-converted modes given in Eq. (7). The detection probability of this state in the image plane (13) is position correlated with the trigger photons in the SLM, giving rise to a ghost image of the chess board pattern with contributions of multiple down-converted modes, as shown in Fig. 3(c) [see also Fig. 5(c)]. With the ICCD in the far field, we measured the diffraction pattern associated with this incoherent sum of spatial modes, shown in Figs. 3(d) and 5(d), which is similar to the intensity distribution of the down-converted light as seen on the camera ICCD [see Fig. 2(b)].

We adjusted the SPDC source intensity to reduce the probability of generating multiple photon pairs within one gate of the intensifier. This was achieved by inserting a neutral density filter in the path of the pump beam and by controlling its polarization. The measured count rates in the object arm were 1.323kHz when using the single-mode fibre and 104.709kHz when using the multi-mode fibre. Both these count rates are compatible with the maximum trigger rate of the ICCD of 500kHz. With the pump laser off, we measured the background-count rate of the SPAD to be approximately 1kHz (see table 1).

4.1. Heralding efficiencies of the camera arm

The heralding efficiencies of the triggered multi-pixel detection system in the camera arm can be estimated from the number of detected photons on the ICCD. After applying threshold photon counting, the pixel outputs of each image acquired over an exposure time of $\tau = 2$s are assigned a value "0" or "1", where "1" correspond to a photo-detection or a noise event [33, 34]. Typical examples of the obtained digitized images are shown in Fig. 6. With the appropriate time-gating of the intensifier, these photo-detection events and those in the SPAD are associated with detections of photons belonging to the same generated pairs [7, 12]. The photo-detections on the CCD chip of an ICCD happen after the amplification of the input photons on the inten-

#198207 - $15.00 USD Received 23 Sep 2013; revised 4 Nov 2013; accepted 4 Nov 2013; published 4 Dec 2013

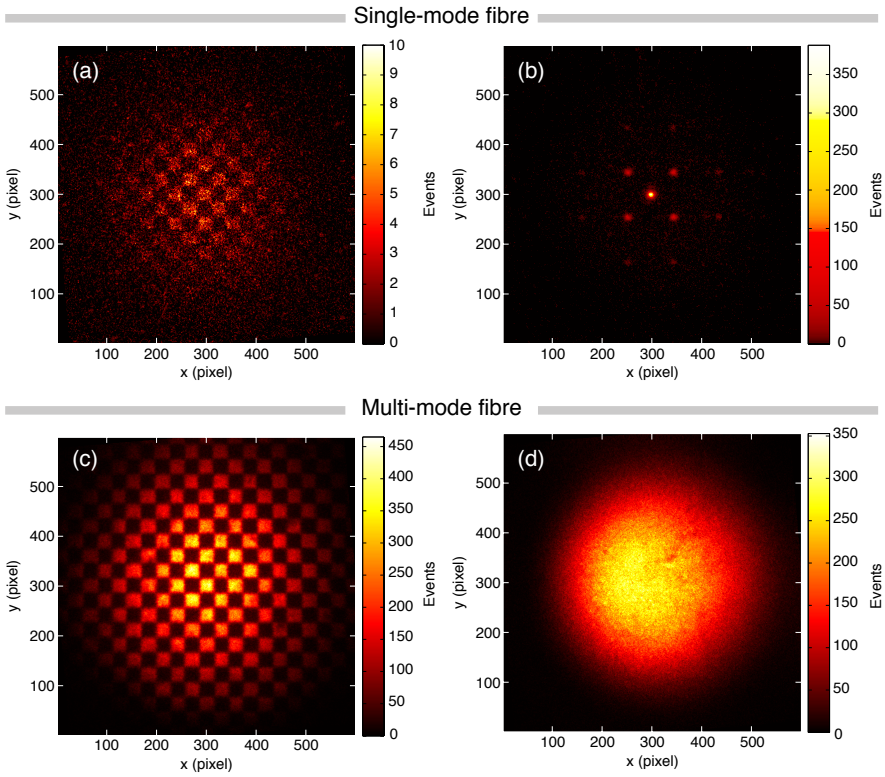

Fig. 3. Triggered images obtained on the ICCD for single-mode, Figs. 3(a) and 3(b), or multi-mode, Figs. 3(c) and 3(d), detection of the trigger photons. The images in Figs. 3(a) and 3(c) where taken with the ICCD in the image plane and the images in Figs. 3(b) and 3(d) with the ICCD in the far-field of the SPDC source. The colormap scale represents the number of photo-detection events in each pixel. Note that the colormap of Fig. 3(b) was adjusted to allow the visualization of the low-intensity features of the diffraction pattern.

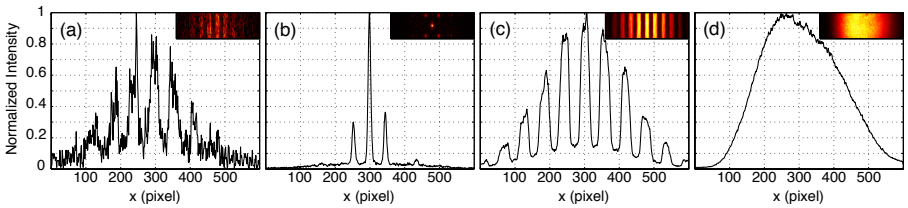

Fig. 4. Summed horizontal cross-sections of the images shown in Fig. 3. The cross-sections were summed over the central 20 rows for the images in image plane and 120 rows for the images in the far-field. The insets show the part of the images used.

sifier. This amplification process spreads the signal resulting from a single photon over neighbouring pixels on the CCD chip, reducing the resolution of the detection mechanism. Thus, a good estimation of the number of detected heralded photons is based on the number of generated photo-detection "islands" rather than the number of photo-detections on the CCD chip [7].

#198207 - $15.00 USD Received 23 Sep 2013; revised 4 Nov 2013; accepted 4 Nov 2013; published 4 Dec 2013

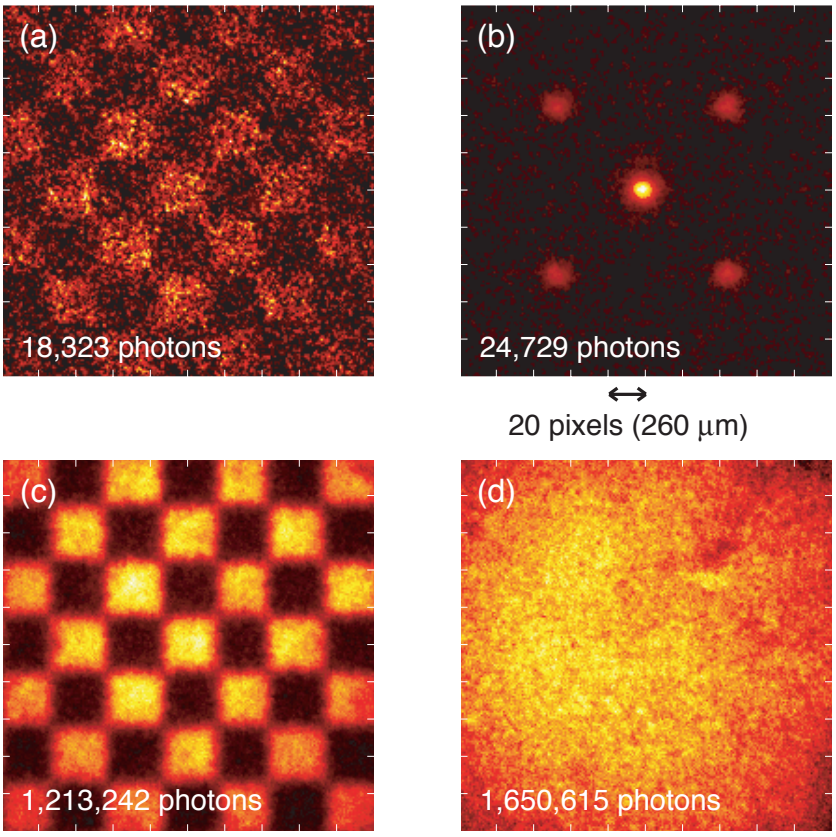

Fig. 5. Close-up showing the central part of the images displayed in Fig. 3. The area of the CCD chip displayed in these images is $(2.6 \times 2.6)\text{mm}^2$. The written number of photons in each of these images was calculated based on the number of photo-detection islands, as explained in section 4.1. Note that the numbers provided for the images with the multi-mode fibre, Figs. 5(c) and 5(d), are an under-estimation of the number of detected photons (see section 4.1).

Using this counting methodology, we calculated the average number of detected events, $\bar{N}_e$, from the 1800 images taken with the single- or multi-mode trigger detection system with the ICCD in the image plane and far-field of the SPDC source. These numbers are summarized in table 1. We note that although a photo-event island is counted as a single detected photon, all excited pixels on the CCD chip contributed to the generated images in Figs. 3 and 5.

From the average number of detected events per image $\bar{N}_e$, we subtract the predicted number of noise events $\bar{N}_n$ to obtain an estimation of the average number of detected heralded photons. The noise probabilities in a single-photon sensitive CCD can be estimated from a series of images acquired with the shutter of the camera closed [33,34]. Using the same settings used for the signal acquisition, we acquired a series of 100 images with the shutter of the ICCD closed. Applying the same counting methodology for these images taken "in the dark", we obtain a prediction for the number of noise events per image (see table 1).

#198207 - $15.00 USD Received 23 Sep 2013; revised 4 Nov 2013; accepted 4 Nov 2013; published 4 Dec 2013

We define the heralding efficiency η_H of the triggered detection system in the camera arm as

$$\eta_H = \frac{\bar{N}_e - \bar{N}_n}{\tau(S_T - S_{BG})}, \tag{15}$$

where S_T and S_{BG} are the trigger and background count rate of the SPAD in the object arm, respectively. The difference of these count rates in the denominator of the heralding efficiency (15) represents the average number of trigger photons per second. As these count rates are expressed in units of s^{-1}, we multiply them by the exposure time τ of the images to obtain the number of trigger events during an exposure of the ICCD. The measured values of these quantities along with the calculated heralding efficiency are summarized in table 1.

The heralding efficiency (15) is the ratio between the average number of detected photons on the ICCD and the average number of trigger photons on the SPAD. Applying Eq. (15) to our set of data, we obtain $\eta_H \approx 3\%$ for the single-mode detection system and $\eta_H \approx 1\%$ for the multi-mode detection system (see table 1). It is perhaps surprising to notice the lower heralding efficiencies obtained for the multi-mode case. This difference, however, is attributed to the higher mean number of photons per image and limitations both in the detection mechanism of the camera and our photon counting methodology. As a photo-event manifest itself as a multi-pixel island of photo-detections on the CCD chip [12, 35], photons arriving in neighbouring pixels within the same acquired image can generate a connected photo-detection island that is counted as a single-photon event with our counting algorithm. In this case, the number of photo-detection islands is no longer a good estimation of the number of detected photons. In the single-mode case, this does not affect the number of photons counted as the image is sparse (see Fig. 6). Therefore, the values for η_H obtained with the data for the single-mode fibre is a better estimate of the heralding efficiency of our system. We note that the significantly higher heralding efficiencies achieved in this work as compared to [7] are due to the utilization of an ICCD with higher quantum efficiency (the quantum efficiency of our photocathode at the wavelength of 710nm is approximately 30%).

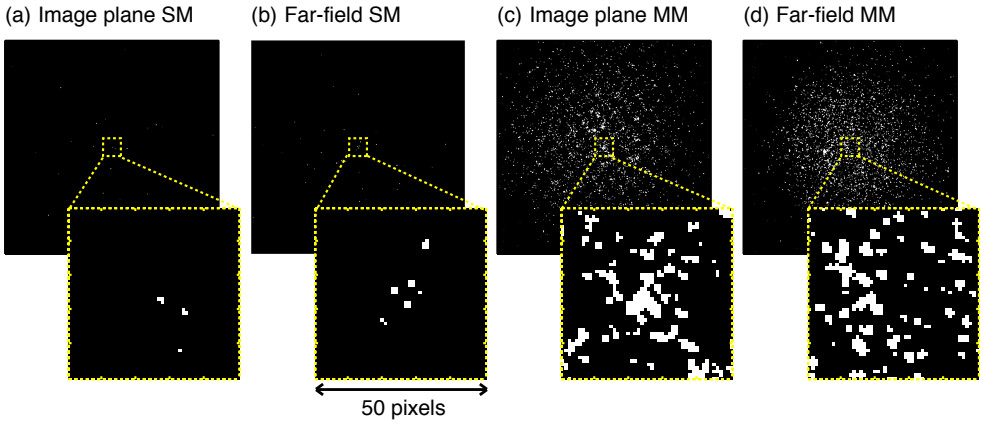

Fig. 6. Example of typical images obtained after digitization of the pixel outputs. The insets show an enlargement of 50×50 pixels of the central part of the images. Photo-detection islands comprising a few adjacent pixels are visible in the images taken with the single mode fibre, Figs. 6(a) and 6(b). Due to the higher mean number of photons, connected photo-detection islands can be seen in the images taken with the multi-mode fibre, Figs. 6(c) and 6(d).

#198207 - $15.00 USD Received 23 Sep 2013; revised 4 Nov 2013; accepted 4 Nov 2013; published 4 Dec 2013

Table 1. Table with the relevant values for the calculation of the heralding efficiencies of our multi-pixel triggered detection system. $\bar{N}_e$: average number of events per image; $\bar{N}_n$: predicted number of noise events per image; S_T: trigger rate (in units of s^{-1}); S_{BG}: background count rate (in units of s^{-1}); η_H: heralding efficiency as defined in Eq. (15). The acquisition time of each image is $\tau = 2$s, and the average number of detected events per image $\bar{N}_e$ is calculated based on the total number of acquired images, 1800.

	Image plane SM	Far-field SM	Image plane MM	Far-field MM
$\bar{N}_e$ (events/image)	32.74	31.34	2052.96	2292.80
$\bar{N}_n$ (events/image)	8.88	8.88	91.43	91.43
S_T (kHz)	1.323	1.323	104.709	104.709
S_{BG} (kHz)	0.966	0.966	1.024	1.024
η_H (%)	3.3	3.1	0.9	1.1

It is important to notice that accidental detections of photons on the ICCD were not taken into account in the calculation of the heralding efficiencies in table 1. In our system, there are two sources of accidental detections of the photons in the camera arm. The first is based on multiple photon pair emissions within one gate time of the intensifier and the second is based on "false" triggers of the ICCD due to dark-counts in the SPAD. These accidental detections are clearly visible in the cross-section shown in Fig. 4(c), where a low background intensity with the shape of the SPDC beam in the image plane [see Fig. 2(a)] is present. As the triggering rate of the intensifier is greater for the multimode detection system, it is expected that a greater number of accidental detections is observed in this case. At the cost of increasing the sampling time required to acquire the images, the number of accidental detections can be reduced by reducing the down-conversion source intensity.

5. Conclusions

Spontaneous parametric down-conversion produces pairs of photons entangled over a wide range of spatial modes. Despite this rich entangled multi-mode structure of the photon pairs, fourth-order correlations are normally measured through the scanning of single-photon detectors across the detection planes. In this paper we used an approach based on a time-gated ICCD camera to obtain fourth-order images and diffraction patterns while observing the full transverse mode structure of the down-converted photons. This full-field coincidence detection system relies on the detection of one of the photons from a pair by a single-photon avalanche diode, the output signal from which is used as a trigger to a time-gated ICCD camera placed in the detection plane of the other photon [7, 12].

Using the ICCD in this triggered configuration, we acquired ghost images and diffraction patterns of an object encoded on a spatial light modulator. Ghost images of the object were obtained both for the single-mode and the multi-mode detection of the trigger photons transmitted through the object. The observation of ghost diffraction patterns, however, required the projection of the trigger photons into a spatially coherent mode. It is interesting to notice that the use a pump laser prepared in a non-Gaussian spatial mode can lead to an anomalous behavour of the visibility of fourth-order diffraction and interference patterns with the detection aperture [10, 11]. Our approach can be utilised in the study of spatial correlations of photons from SPDC, particularly in fourth-order imaging techniques [13–17] and in the characterization of heralded single photon states such as in remote state preparation [25, 26].

#198207 - $15.00 USD Received 23 Sep 2013; revised 4 Nov 2013; accepted 4 Nov 2013; published 4 Dec 2013

Acknowledgments

This work is supported by EPSRC (EP/I012451/1) and Hamamatsu. M.J.P. thanks the Royal Society, the Wolfson Foundation and the US DARPA/DSO InPho program. R.W.B acknowledge the financial support from CERC. We acknowledge financial support by the European Commission via the FET Open grant agreement Phorbitech FP7-ICT-255914. We would like to thank P. H. Souto Ribeiro for the careful reading of this manuscript.

#198207 - $15.00 USD Received 23 Sep 2013; revised 4 Nov 2013; accepted 4 Nov 2013; published 4 Dec 2013